Optical Engineering 49(2), 023602 (February 2010)

# Common-path two-wavelength interferometer with submicron precision for profile measurements in on-line applications

**José María Enguita**
**Ignacio Álvarez**
**María Frade**
University of Oviedo
Department of Electrical Engineering
Campus de Viesques
Gijón, Asturias 33204 Spain
chema@isa.uniovi.es

**Jorge Marina**
DSIPlus, Cirujeda
12 Bajo
33205 Gijón, Spain

**Abstract.** We propose a common-path two-wavelength interferometric system based on a single optical element, a Savart plate, that is able to obtain single-shot profile measurements with submicron precision from safe working distances (beyond 100 mm). These characteristics make this sensor ideal for surface inspection in on-line applications. For the illumination branch, two lasers with close wavelengths are combined and then passed through a rotating holographic diffuser for drastic speckle reduction. In the acquisition branch, the interferometric signals of both wavelengths are captured simultaneously by a camera, and their phase signals are combined to extend the measurement range.  [DOI: 10.1117/1.3321709]

Subject terms: profiling; shearing interferometry; Savart plate; phase measurement; multiple-wavelength interferometry.

Paper 090588PR received Aug. 3, 2009; revised manuscript received Dec. 8, 2009; accepted for publication Jan. 5, 2010; published online Feb. 23, 2010.

## 1 Introduction

Characterization of surface profiles with submicron precision in industrial environments is crucial for surface inspection and quality control in many industries such as steel or ceramics. Surface defects, as well as the overall shape of the surface, determine its quality; flatness, waviness, or roughness, for instance, are important parameters for quality assessment,[1] and they usually have to meet strict requirements. In these cases, on-line measurement of the surface topology in the production line would result in evident benefits in quality control and process feedback.

As is well known, common-path interferometric systems are ideal for on-line industrial applications due to their simplicity, high stability, low cost, and immunity against vibrations and harsh environmental conditions (see for instance Ref. 2).

Our system is based on shearing interferometry and resembles conoscopic holography,[3] but uses a Savart plate as a shearer instead of a conoscope, as suggested by Haüsler et al.[4] The setup includes triangulation between the illumination and detection branches, so that not only the frequency but also the phase of the resulting signal depends on the distance between the detection plane and the light emitting point. By measuring the phase instead of the fringe frequency, resolution is increased by at least one order of magnitude.[5]

As laser light is used as illumination, the system is affected by speckle noise. Reducing speckle to increase precision is required in this kind of system, and has already been addressed in Ref. 6. Adding speckle reduction resulted in measurements with precision below one micron from working distances beyond 100 mm.

However, an additional problem arises in this case. The use of the phase information reduces the maximum steep that can be measured without ambiguity, as it is only possible to obtain correct measurements when the distance steeps are below half the period of the interferometric signal. With current setups, which provide high resolutions, this means that steeps as small as one micron may be incorrectly measured, which in turn might become unacceptable for most applications (except maybe for mere defect detection). This is a common problem with all phase-measurement techniques, as the phase values are limited to the interval $[0,2\pi)$.

A possible technique to overcome this limitation is based on the use of more than one wavelength,[7–10] so that the unambiguous region is extended to half the equivalent wavelength, which can be calculated as:

$$\lambda_{eq} = \frac{\lambda_1 \lambda_2}{|\lambda_2 - \lambda_1|}. \quad (1)$$

Thus, the use of closer wavelengths provides a higher range and less sensitivity to chromatic aberrations, but noise is also amplified, as it is also scaled by a factor inversely proportional to the wavelength difference. There have been some attempts to minimize this effect (see for instance Ref. 7). Another issue that usually limits the proximity of these wavelengths is that it might be difficult to separate correctly the information from both signals in the presence of noise or, alternatively, to extract the phase information at the synthetic equivalent wavelength $\lambda_{eq}$ as its-related frequency peak in the spectrum may lie too close to the low frequencies, and therefore can be difficult to distinguish from noise caused, for instance, by uneven illumination. Although well known from some time, there is still a lot of research and development in the area of two- and

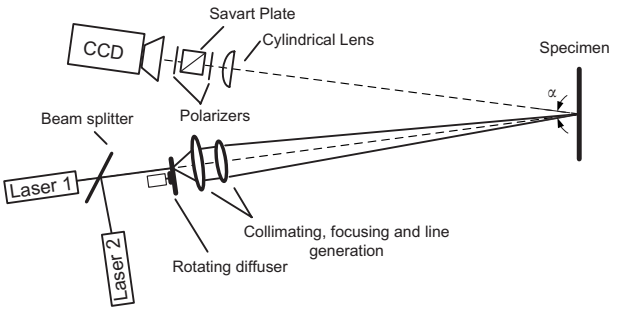


**Fig. 1** Schematic working principle of the two-wavelength interferometer prototype.

multiple-wavelength interferometry to extend the unambiguous range in the measurement of height steps of discontinuous objects.[11,12]

Our approach combines two laser sources of different wavelengths and passes the resulting beam through a rotating holographic diffuser to reduce speckle noise. A laser line is projected onto the object under inspection, and the Savart plate, sandwiched between two polarizers, divides the reflected wavefront in two (corresponding to ordinary and extraordinary rays), which interferes in the detection plane. A cylindrical lens is used to obtain the signal corresponding to the whole profile in a single frame (see Fig. 1).

In the resulting signal, the beat phenomenon (a typical low frequency envelope that appears when two sinusoidal signals are combined) is observed. Two peaks, one associated with each wavelength, appear in the frequency domain, making it possible to extract both phase signals from a single pattern. These phase signals can be combined to increase the maximum slope measurable without ambiguity.

In this work the theoretical background of this system is outlined, the signal processing is discussed, and experimental results with a laboratory prototype are analyzed. Currently, we have obtained submicron precision from distances beyond 100 mm in profiles 12 mm long, but the system is easily scalable to meet other application requirements. Also, phase objects should be measurable with a convenient reference surface.

## 2 Working Principle

Figure 1 shows the schematic diagram of the dual-wavelength interferometer based on a Savart plate. The experimental prototype sensor consists of two lasers of 685 and 660 nm with powers of 50 and 100 mW, respectively, with external power control. In this way it is possible to adjust the power of the individual lasers so that two clear peaks about the same amplitude appear in the frequency spectra. Also, it is simple to adapt the power according to the reflective properties of the surface, and to use just one of the wavelengths if necessary.

The wavelengths are chosen so that they are close enough to provide an important improvement in the measurement range over the individual phase signals, while still being correctly identified in the frequency domain when performing signal processing. Both the illumination and acquisition branches work at a distance of 100 mm from the test specimen, which is mounted on a precision stage (not shown) with lateral movement for 3-D scanning.

Both incident beams are combined together in a beamsplitter and passed through a rotating holographic diffuser with a small diffusion angle (0.5 deg). This provides better performance than usual ground-grit diffusers. There are less power losses and the resulting beam is easier to focus, while still providing good speckle reduction. The resulting beam is transformed into a line by a line generation lens, and projected onto the inspected sample.

The reflected light is passed though a Savart plate, which is made up of two birefringent crystals of equal thickness cemented together and rotated 90 deg with respect to each other. An incident beam propagating through the first crystal is divided into ordinary and extraordinary beams displaced from each other. In the second crystal, the ordinary beam becomes an extraordinary beam, and vice-versa. The result is two emerging beams displaced along a diagonal. This displacement, or shear, can be calculated as 0.075 times the total thickness of the plate if they are manufactured with calcite, which is the case in this prototype. We use a Savart plate with a thickness of 7 mm, which provides a total shear of 0.525 mm.

### 2.1 *Fringe Formation for a Single Source*

If the Savart plate is sandwiched between two polarizers aligned at 45 deg to the optical system, an input beam produces a set of parallel fringes in the detection plane. The density (or frequency) of these fringes varies linearly with the distance between the detection plane and the light-reflecting point. This frequency $f$ follows the equation:

$$f = \frac{s}{\lambda z}, \tag{2}$$

where $s$ is the shear, $\lambda$ is the wavelength of the source, and $z$ is the distance between the specimen and the observation plane. Due to the triangulation in the setup, fringes are also shifted due to the apparent lateral displacement with distance variations. Therefore, not only the frequency but also the phase carries information on this distance, so the equation that defines the interference signal is as follows:

$$I = I_0\left\{1 + \gamma_0 \cos\left[2\pi\frac{s}{\lambda z} + \varphi(z)\right]\right\}, \tag{3}$$

where $\gamma_0$ is the fringe visibility and $\varphi(z)$ is the phase, which varies almost linearly with distance $z$.

To obtain the measurement of a whole profile in each frame, our system projects a laser line over the specimen. A cylindrical lens is used to record a fringe pattern in which each line in the charge-coupled device (CCD) contains the interference signal for a point in the profile. Thus, by measuring the phase of the cosine signals in each of the CCD lines, it is possible to obtain relative distance variations in the profile with at least ten times more precision than using the frequency, as has been shown in Refs. 5 and 13–15.

### 2.2 *Dual-Wavelength Setup*

In this interferometer, the individual effective wavelengths that define the maximum measurable steep (the distance for which a $2\pi$ jump occurs in the phase signal) do not only

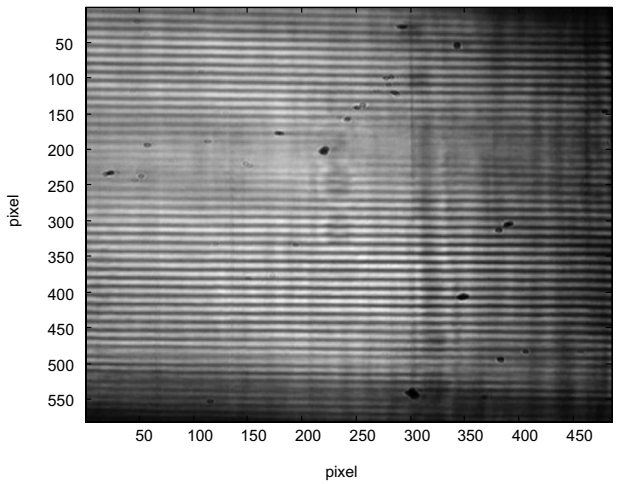


**Fig. 2** Obtained fringe pattern for the two-wavelength system.

depend on the wavelength of the illuminating source, but also on the triangulation angle and the fringe frequency.

The triangulation angle might be difficult to modify physically with precision, so it does not seem to be a good approach. The fringe frequency can be varied by using two Savart plates of different thicknesses. By having different fringe spacing, the same lateral displacement due to distance variations is translated into a different amount of shift in the phase angle, providing the resulting effective wavelengths we are looking for. However, the final system might be complex, and data-matching problems may arise.

Another alternative is using two wavelengths in the illuminating source, which is simpler, and so it is the approach used in this prototype. This setup provides one single pattern in which the beat phenomenon is observed. In the modulus of the Fourier transform of each column, two peaks appear, one associated with each wavelength, making it possible to extract both phase signals.

We use a $1280 \times 1080$-pixel CCD camera rotated 90 deg to maximize the lateral resolution along a profile, which is approximately 10 $\mu$m per pixel. Each column in the resulting pattern contains the cosine interference signal for each pixel along the profile. The obtained fringe pattern is shown in Fig. 2, where the beat phenomenon appears. This is clearer in Fig. 3, where one of the columns of the fringe pattern is plotted. The frequency spectrum of this line (shown in Fig. 4) clearly shows two peaks with maxima at indexes 343 and 331. The ratio between those maxima (1.0363) strongly agrees with the nominal ratio between the laser wavelengths of 685 and 660 nm (1.0379).

It is possible to calculate the improvement factor $I_f$ in the measurable range in terms of the ratio between both wavelengths, as shown in Eq. (4). In our case, this factor is slightly larger than 27.

$$I_f = \frac{\lambda_1/\lambda_2}{|1-\lambda_1/\lambda_2|}. \tag{4}$$

### 2.3 *Error Sources*

By using close wavelengths and getting their data set simultaneously, some common sources of error outlined by Cheng and Wyant[7] are reduced. 1. The phase fluctuation introduced by air turbulence is reduced by the use of two close wavelengths if their phase fronts are taken from the same fringe pattern.[16] 2. There are no data matching problems. 3. Chromatic variations of the wavefront aberration introduced by the optical system affect similarly at both wavelengths, so they almost cancel each other.

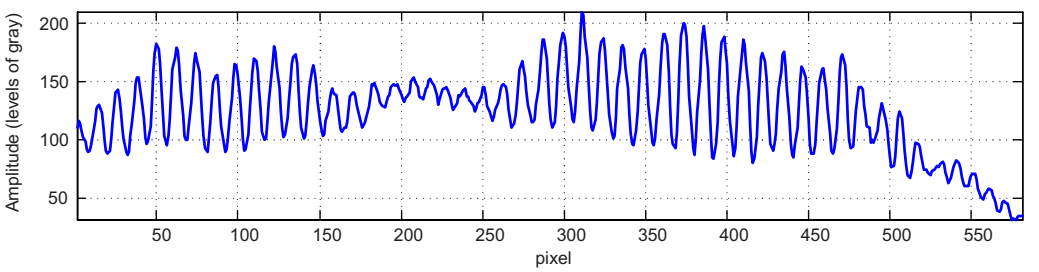


**Fig. 3** Obtained signal corresponding to column 100 in the pattern of Fig. 2. A low-frequency beat phenomenon is observed. (Color online only.)

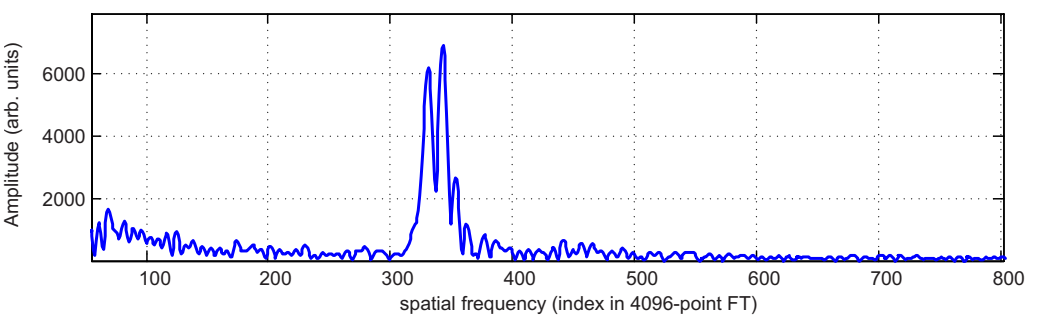


**Fig. 4** Detail of the 4096-point Fourier transform of the signal in Fig. 2. Two peaks at indexes 331 and 343 appear clearly. (Color online only.)

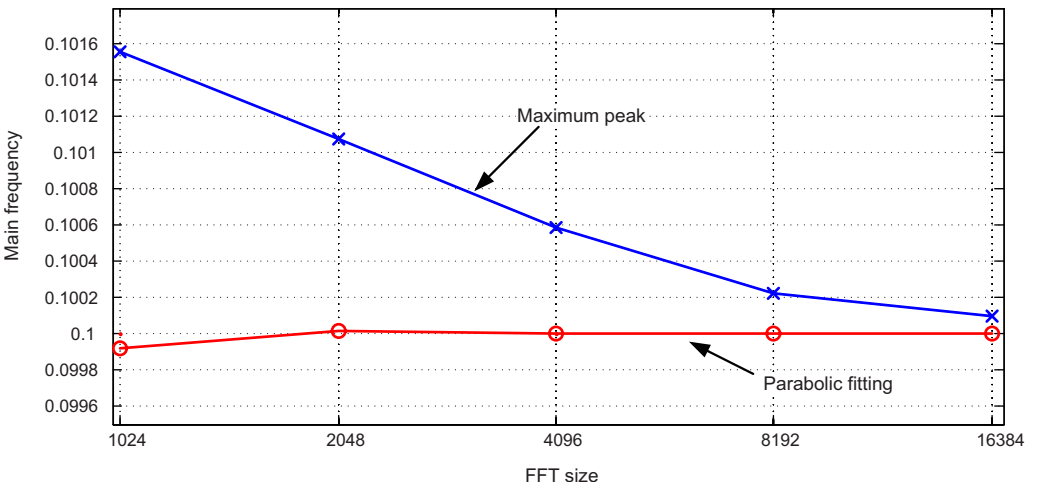


**Fig. 5** Performance of the parabolic fitting to find the main frequency. The input signal is a cosine of frequency 0.1 cycles per pixel. (Color online only.)

Nevertheless, other sources of error still exist and may cause problems. 1. There is an observed nonlinearity in the system, caused mainly by the optical elements. For instance, small thickness variations in the manufacturing of the Savart plate introduce differences in frequency along the profile for a flat reference sample (a silicon wafer), and also variations in the obtained phase front. However, this should not pose a big problem for the calibration task. 2. The Savart plate produces a copy of the wavefront with a lateral shear without introducing a phase difference only for normal incidence. If light incides at a given angle, a sinusoidal phase variation appears and is superimposed to the actual phase front. False height variations due to this effect have a long spatial wavelength, which is usually filtered out before performing any roughness analysis or defect detection, if they are not removed by the calibration process. 3. The rotating diffuser also introduces errors in the measurement that are added to the general camera noise, loss of light, and reflections, among others. 4. Both lasers should be correctly aligned so that the two generated lines are superimposed, otherwise both phase fronts may not correspond exactly to the same profile.

These effects may cause errors in the obtained phase, which will be magnified by a factor inversely proportional to the wavelength difference. This seems to be a common problem for all two-wavelength techniques.[7]

## 3 Signal Processing

There are two alternatives for extracting the phase signal at the equivalent synthetic wavelength $\lambda_{eq}$, but both heavily rely on accurately finding the index of the maximum in the modulus of the Fourier transform for each interference signal (column). The resulting phase values are the values of the angle of the Fourier transform at those indexes. For increasing this accuracy, once the maximum inside a search window is found, the real value is calculated as follows.

1. Consider $i$ the index of the maximum and $v_i$ the value of the modulus of the Fourier Transform at index $i$.
2. Use the pairs $(i-1, v_{i-1})$, $(i, v_i)$, $(i+1, v_{i+1})$ to perform a parabolic fitting.
3. Get the derivative of the resulting polynomial. Its root is the new, more accurate index $\hat{i}$.
4. Do the same parabolic fitting for the unwrapped angle values and evaluate the polynomial at $\hat{i}$. Alternatively, calculate the value of the discrete Fourier transform (DFT) at $\hat{i}$ and take the angle. This is the value of the phase.

This method could find the correct frequency using even less points in the Fourier transform. For instance, our current processing software uses a 4096-point Fourier transform, but we have experimentally proved that using a 2048-point transform with the previous method results in identical values for the obtained phase front. Figure 5 shows the performance of this method using a cosine input signal of 0.1 cycles per pixel. The plots show the frequency obtained directly as the maxima of several fast Fourier transforms (FFTs) of different numbers of points, and after applying the parabolic fitting.

This process should be done for every column in the fringe pattern to obtain the phase value associated to the whole profile. The two alternate methods differ on which frequency is analyzed: the synthetic frequency (due to the beat phenomenon) or the two frequencies corresponding to the individual wavelengths.

### 3.1 *Obtaining the Phase at the Beat Frequency*

It is possible to work directly with the information at the beat frequency, as it is done in Ref. 12. The phase can be calculated as the angle of the Fourier transform at that frequency, as long as it is separable from other lower frequencies (mainly zero). Figure 6 shows this frequency in our prototype. As the two wavelengths are close, this frequency is very low, and the search window for the proposed algorithm should be very small. This leads to errors in the presence of noise, and also prevents the use of the equivalent wavelength phase data to correct the $2\pi$ ambiguities in the single-wavelength data, as proposed by Cheng and Wyant,[7] as a way to reduce the noise amplification effect discussed before.

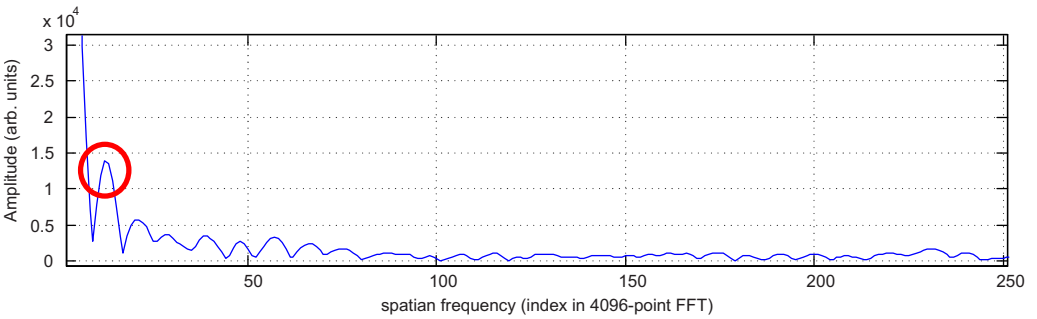


**Fig. 6** Detail of the 4096-point Fourier transform of the signal showing the frequency of the beat. (Color online only.)

### 3.2 *Obtaining the Phase at Individual Wavelengths*

In addition to the peak at the beat frequency, the individual wavelengths produce peaks at higher frequencies. As long as they can be correctly separated, this information can be used to extract the individual phase from the same interference signal.

As it was already shown in Fig. 4, two clear different peaks appear in the frequency spectrum, one associated with each laser wavelength. This is an important difference between this technique and others in which a single peak at the average wavelength is found, because it removes the need of performing different acquisitions, one for each wavelength, or one with both wavelengths to be processed at the beat frequency, and another with a single wavelength to provide better performance in the final measurement.

To obtain the individual phase data, one possible procedure is to search for the maximum in the frequency spectrum (inside a window), get the phase value, filter out that frequency (and a small window around it), and repeat the process to obtain the phase value for the second wavelength. The resulting values should be reordered based on the index found, if necessary, as the first maximum does not necessarily correspond to the same wavelength all the time.

Also, to make the processing more robust, it can take into account the fact that the ratio between both indexes should be constant and equal to the ratio between wavelengths. Once the highest peak has been found, we can search for the second at given positions (practically a small window) at the left or right of that peak. In addition, the difference between the ratio of the calculated maxima and the nominal ratio can be used as a measurement of the quality of the signal. Local errors can be solved (or at least, filtered out) if this magnitude falls below a given threshold.

Once the two phase fronts $\varphi_1(x)$ and $\varphi_2(x)$ have been extracted, the phase at the synthetic wavelength $\phi(x)$ can be obtained by simple substraction:

$$\phi(x) = \varphi_1(x) - \varphi_2(x). \tag{5}$$

Repeatability is quite high along the whole profile. Measuring 15 consecutive acquisitions shows an average standard deviation of $\sigma < 0.04$ $\mu$m.

## 4 Experimental Results

We performed several experiments to test the behavior of the prototype shown in Fig. 1. We have not performed a complete calibration task, but we have experimentally calculated a conversion factor between the phase angle in radians and the height in microns using reference patterns.

In the first experiment, the prototype was used to perform a scanning of two reference objects made of bands of resin over a silicon wafer substrate. These bands are one millimeter wide and (approximately) one micron high, with separations of two millimeters for the first specimen and one millimeter for the second. Figure 7 shows the resulting surface map for the first specimen. A small scratch over the wafer can be seen in one of the borders, as well as other smaller surface defects. Also, the effects of light diffraction are observed. Figure 8 shows the phase maps for the second specimen and how the dual-wavelength system solves the ambiguities that can be noticed in the single-wavelength phase maps (where steps sometimes appear inverted or are hardly noticeable).

In the second experiment, the target surface was a Rubert Company ( Cheshire, United Kingdom) 511 reference

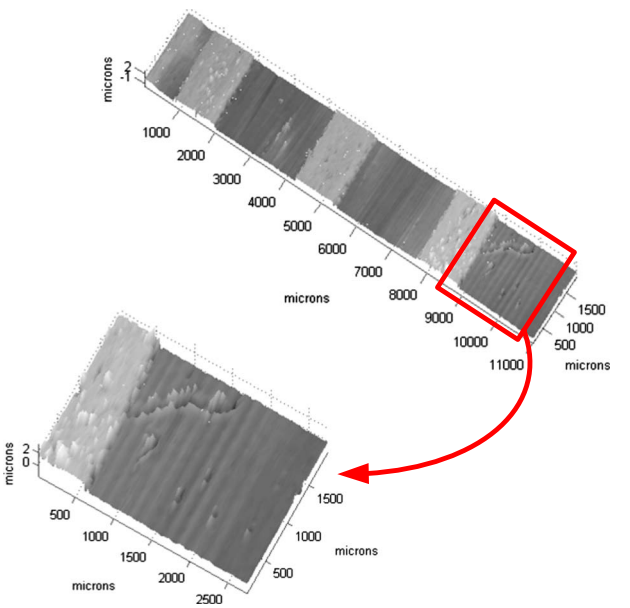


**Fig. 7** The result of scanning a test object with bands of resin over silicon with heights of one micron and widths of one millimeter with separations of two millimeters. Small inclusions and dust can create diffraction patterns over the obtained surface, which are observable near the scratch. (Color online only.)

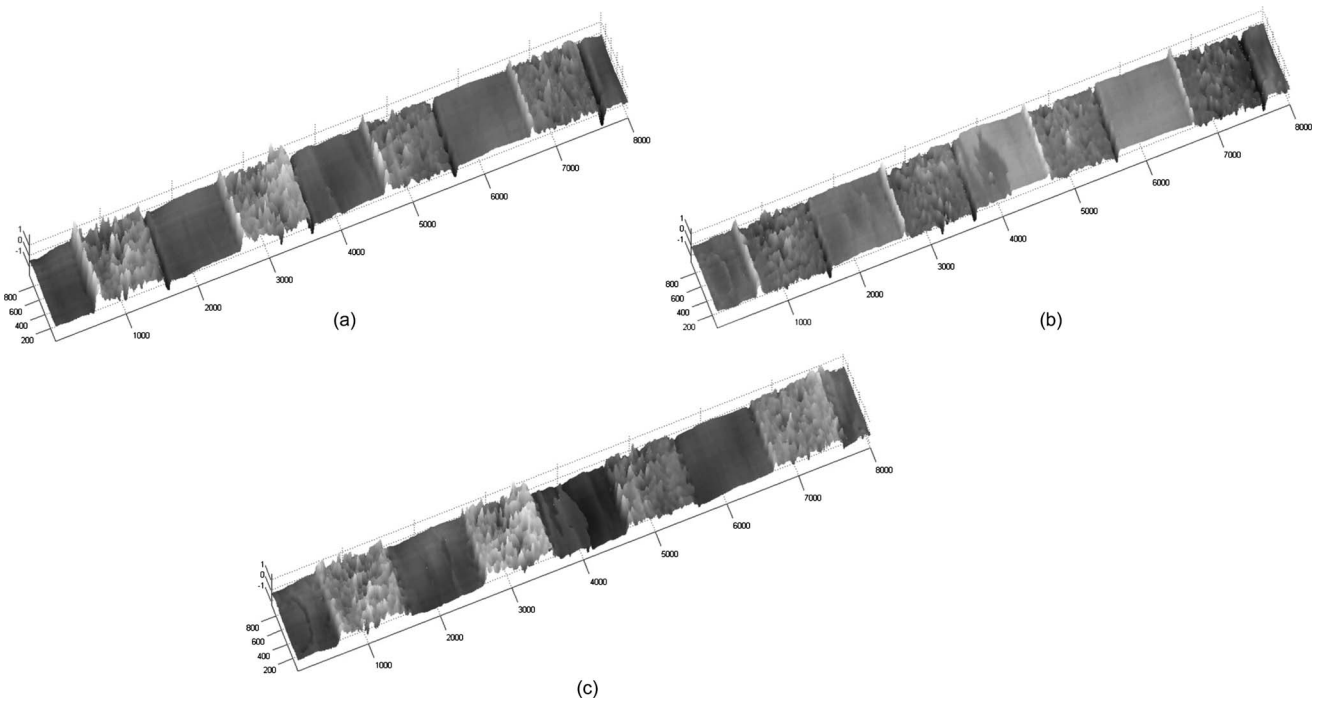


**Fig. 8** Raw phase maps obtained for a test specimen with steps of one micron. Plots (a) and (b) show the phase maps for the individual wavelengths, while (c) shows the combined phase map at the equivalent wavelength. *x* and *y* axes are in microns, while *z* is in radians.

specimen consisting of a single groove with a depth of one micron and 100 $\mu$m wide. Figure 9 shows detail of the resulting obtained profile, where the groove is clearly observed.

Also, a Rubert Company 531 test specimen was scanned. This sample consists of a sinusoidal surface with an amplitude of one micron and a period of 100 $\mu$m. Detail of the obtained surface map is shown in Fig. 10. This surface map is quite noisy due to reflections, but the overall shape and dimensions are correctly obtained. By using just the part of the resulting map with lower noise, the roughness parameters can be calculated according to ISO 4287 and compared to the nominal ones (cut off at 0.8 mm) provided by the manufacturer. Results are shown in Table 1. Mean values agree, but standard deviations are higher due to the presence of noise. This kind of experiment would benefit from more sophisticated filtering techniques, but serves to show the behavior of the sensor, even in this limiting case.

Finally, a mirror was scanned for surface defects and results were checked with a microscope. Figure 11 illustrates this experiment. Phase errors appear at the borders of the defects when the laser line hits them as the sample moves in the scanning process. This is probably due to light scatter or diffraction effects. However, the shapes are quite correct and the presence of even very small defects is correctly detected. No postprocessing has been applied to this phase map.

## 5 Discussion

Although results are promising, there are still some points and limitations that should be addressed. First, one of the more delicate parts of the system is the line generation, as it is difficult to obtain a thin, well-focused line that is needed to obtain fringes of good contrast. The main reason is the speckle reducing system based on a rotating diffuser. More sophisticated methods will be studied in the future, as well as the use of other kinds of noncoherent light.

The system is also quite asymmetric, providing very high precision in depth measurements (below the micron) but only about 10 $\mu$m of lateral resolution (along the profile). This can be enhanced by using a different type of lens

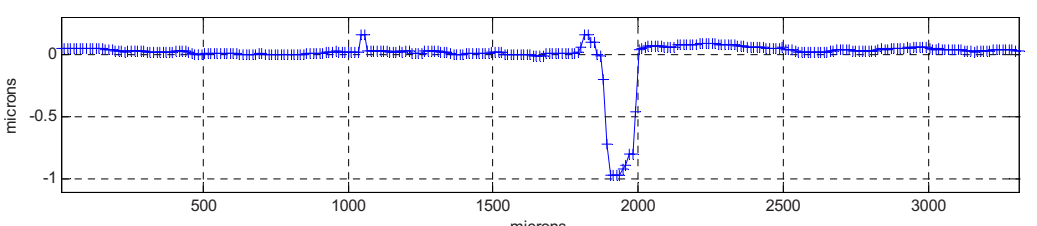


**Fig. 9** Profile of Rubert specimen 511. This specimen consists of a single groove of one micron. (Color online only.)

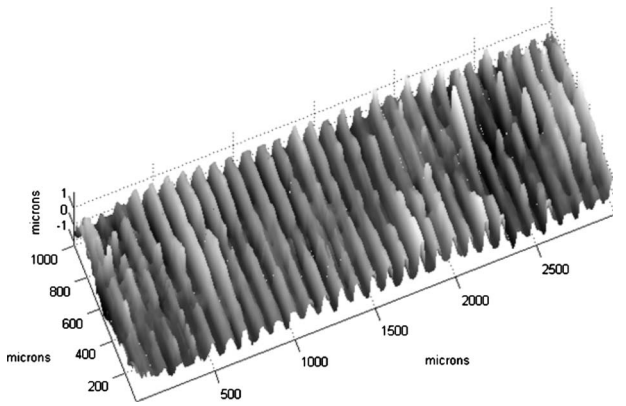


**Fig. 10** Detail of the scanning of Rubert specimen 531, a sinusoidal pattern of amplitude one micron and a period of 100 $\mu$m.

**Table 1** Comparison between $R_a$ and $R_z$ factors in microns calculated using our optical sensor and the data provided by the manufacturer.

| Parameter | Manufacturer ($\mu$m) | Our sensor ($\mu$m) |
|---|---|---|
| $\overline{R_a}$ | 0.3175 | 0.316124 |
| $\overline{R_z}$ | 1.022 | 1.070571 |
| $\sigma R_a$ | 0.00123 | 0.053190 |
| $\sigma R_z$ | 0.018 | 0.154289 |

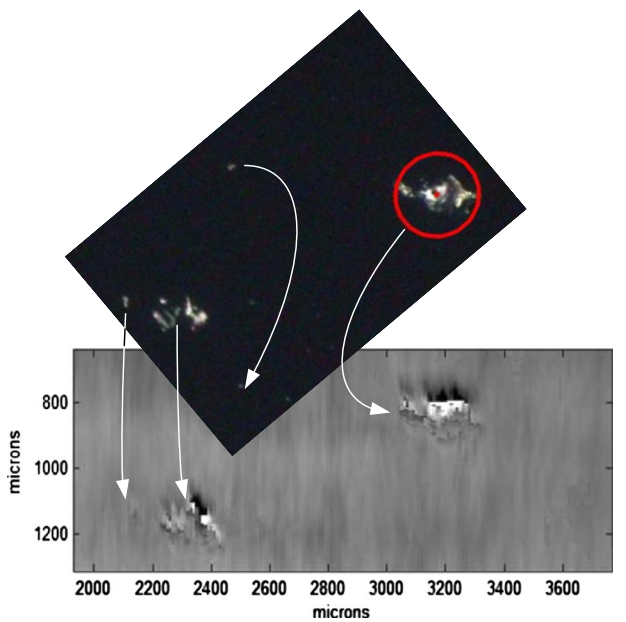


**Fig. 11** Comparison between the obtained phase map without any postprocessing (bottom) and the image obtained by a microscope (top). The latter was rotated to match the orientation of the scanned surface. The red circle on the microscope image has a radius of 135.5 $\mu$m. (Color online only.)

in the acquisition branch (such as macros), but could normally mean also reducing the working distance.

Diffraction is another source of error. The phase would experience variations at any sharp border of the surface due to this effect. This can alter measurements, usually creating false peaks and valleys at those borders. We have seen what seems to be Airy disks in the obtained surface maps from a flat silicon wafer due to very small defects (inclusions, scratches, or dust, for instance). However, this effect can even be helpful in a system aimed at the detection of small surface defects.

Finally, although its impact in the measured profiles was low in these experiments, the effect of a sinusoidal variation in the phase occurring when the light incidence is not normal to the Savart plate needs to be taken into consideration. Usually this will happen due to misalignments in the optical components. The resulting erroneous height variations along the surface map will exhibit low amplitude and a low spatial frequency, which is filtered for roughness analysis or microdefect detection. This variation could also be compensated (at least partially) in the calibration stage.

We have followed the approach of Häusler et al. given in Ref. 4 and used a Savart plate, but similar results could be achieved by other shearing methods.

## 6 Conclusion

In conclusion, we built a prototype of a common-path interferometer able to obtain a 12-mm profile of a target in a single frame with submicron precision and from working distances larger than 100 mm. By using the combination of two lasers of different wavelengths, the measurable range is extended and some error sources are minimized. The beat formation phenomenon is observed experimentally, and the possibility of obtaining the two phase signals from the same fringe pattern is shown. The prototype is used to obtain the surface map of several different objects to verify its capabilities. The repeatability of the measurements is quite high, with a standard deviation below 0.04 $\mu$m.

The main advantages of this system are those of common-path interferometric methods: low sensitivity to environmental perturbations, easy setup, and applicability to a wide range of surface inspection problems. In addition, it is capable of obtaining a distance profile in a single shot at frame rate, making it a good choice for on-line inspection.

### *Acknowledgments*

The authors would like to thank the Ministerio de Ciencia e Innovación of Spain, who supported and funded this work (research project reference DPI2007-64243).

### *References*

1. J. Raja, B. Muralikrishnan, and S. Fu, "Recent advances in separation of roughness, waviness and form," *Precis. Eng.* **26**(2), 222–235 (2002).
2. S. Mallick and D. Malacara, "Common-path interferometers," Chap. 3 in *Optical Shop Testing*, 3rd ed., pp. 97–ss, Wiley-Interscience, New York (2007).
3. G. Y. Sirat and D. Psaltis, "Conoscopic holography," *Opt. Lett.* **10**(4), 4–6 (1985).
4. G. Häusler, J. Hutfless, M. Maul, and H. Weissmann, "Range sensing based on shearing interferometry," *Appl. Opt.* **27**, 4638–4644 (1988).
5. J. M. Enguita, I. Álvarez, C. Fraga, J. Marina, Y. Fenández, and G. Sirat, "Conoscopic holography-based long-standoff profilometer for surface inspection in adverse environment," *Opt. Eng.* **45**(7), 073602

(2006).
6. I. Álvarez, J. M. Enguita, J. Marina, and C. Fraga, "On-line submicron profile measurements from safe distances with conoscopic holography: feasibility and potential problems," *Opt. Eng.* **47**(2), 023602 (2008).
7. Y. Y. Cheng and J. C. Wyant, "Two-wavelength phase shifting interferometry," *Appl. Opt.* **23**(24), 4539–4543 (1984).
8. Y. Y. Cheng and J. C. Wyant, "Multiple-wavelength phase-shifting interferometry," *Appl. Opt.* **24**(6), 804–807 (1985).
9. K. Creath, Y. Y. Cheng, and J. C. Wyant, "Contouring aspheric surfaces using two-wavelength phase-shifting interferometry," *J. Mod. Opt.* **32**, 1455–1464 (Dec. 1985).
10. K. Creath, "Step height measurement using two-wavelength phase-shifting interferometry," *Appl. Opt.* **26**(14), 2810–2816 (1987).
11. U. P. Kumar, B. Bhaduri, M. P. Kothiyal, and N. Krishna Mohan, "Two-wavelength micro-interferometry for 3-D surface profiling," *Opt. Lasers Eng.* **47**, 223–229 (Feb. 2009).
12. D. S. Mehta, P. Singh, M. S. Faridi, S. Mirza, and C. Shakher, "Two-wavelength lateral shearing interferometry," *Opt. Eng.* **44**(8), 085603 (2005).
13. F. Obeso, L. Sancho, I. Álvarez, A. Díez, G. Sirat, and R. Falessi, "Novel on-line surface quality-control for hot slabs in continuous casting," *La Revue Metallurgie* **3**, 267–275 (2002).
14. I. Álvarez, G. Sirat, C. Fraga, J. Enguita, Y. Fernández, and J. Marina, "On-line defect detection with the long stand-off conoline profilometer," *2nd Intl. Conf. Metrol.*, pp. 84–89 (2003).
15. I. Alvarez, I. Díaz, and Y. Malet, "Dimensional control of h-shaped steel beams with conoscopic holography based profilometers," in *Proc. 7th European Conf. Nondestructive Test.* **3**, 8 (1998).
16. L. Zeng, K. Seta, H. Matsumoto, and S. Iwashaki, "Length measurement by a two-colour interferometer using two close wavelengths to reduce errors caused by air turbulence," *Meas. Sci. Technol.* **10**, 587–591 (1999).

**José María Enguita** received his MS degree in computer engineering in 1997 and his PhD from the University of Oviedo (Spain) in 2004, where he is currently working as an assistant professor in the electrical engineering department. His research interests include computer vision and conoscopic holography applications for on-line quality control, both dimensional and surface defects. He has participated in numerous projects in this field, mainly for the steel industry.

**Ignacio Álvarez** received his PhD in industrial engineering in 1997 from the University of Oviedo (Spain), where he is currently working as a professor in the electrical engineering department. His research interests include computer vision and conoscopic holography applications for on-line quality control, both dimensional and surface defects. He has participated in numerous projects in this field, mainly for the steel industry. He has cooperated with Optimet in developments around conoscopic holography since 1994.

**María Frade** received the MS degree in industrial engineering in 2008 from the University of Oviedo (Spain), where she is currently working toward her PhD. She has been working in applications of automation and quality control for the steel industry since 2005. Her current research interests are conoscopic holography, computer vision, and industrial automation.

**Jorge Marina** received the MS degree in industrial engineering in 2003 from the University of Oviedo (Spain), where he is currently working toward his PhD. He is currently working as an engineer at DSIPlus. His research interests are conoscopic holography, computer vision, and industrial automation.